Parametric Study of Urban Microclimate Based on a Coupled Approach for CFD, Radiation, Wind-Driven Rain and Heat and Moisture Transport in Building Materials

Aytaç Kubilay[1], Dominique Derome[1], Jan Carmeliet[1,2]

[1]Laboratory for Multiscale Studies in Building Physics, Swiss Federal Laboratories for Materials Science and Technology (Empa), Dübendorf, Switzerland

[2]Chair of Building Physics, Swiss Federal Institute of Technology ETHZ, Zurich, Switzerland

Abstract

Thermal and moisture capacities of different materials can influence the thermal comfort in urban areas significantly. This study presents a fully-integrated urban microclimate model, which considers the transport of heat and moisture in the air and in building materials, solving also for solar and thermal radiative exchange as well as wind and wind-driven rain. The proposed approach yields detailed analysis of the influence of different materials and meteorological conditions (wind, sun, rain) on the absorption and storage of heat and moisture in the built environment. The case study of the impact of rain deposition on an isolated three-dimensional street canyon shows limited evaporative cooling potential for concrete compared to bare soil.

Introduction

Increase in urban heat island effect has adverse effects on thermal comfort and health as well as causes increase in energy use for space cooling and in greenhouse gas emissions (Moonen et al. 2012). Considerable amount of research is performed with the aim to decrease the causes that lead to urban heat island, based on field or laboratory measurements and computational fluid dynamics (CFD) simulations (Mirzaei and Haghighat 2010; Toparlar et al. 2015). The advantages of CFD are its ability to provide accurate spatial and temporal information and the given possibility to perform parametric studies based on different scenarios. On the other hand, CFD simulations are complex and demanding to perform, which often lead to considerable simplifications in the physics involved in microclimate studies, e.g. storage and redistribution of heat and moisture.

Building materials that are commonly used in the built environment, e.g. concrete, asphalt or brick, play an important role in the absorption, transport and storage of heat and moisture. Such materials can increase sensible heat storage and absorption of short-wave radiation due to increased reflections and use of low-albedo materials and decrease evapotranspiration in urban areas. In addition, moisture storage and distribution within the built environment complicatedly influence the microclimatic conditions, as moisture is the key agent of evaporative cooling, as well as affecting the thermal capacity and conductivity of building materials.

Furthermore, these effects on the urban microclimate are inherently tridimensional.

The present study uses a fully-integrated microclimate model that takes into account the interactions between various physical phenomena and models the three-dimensional redistribution of heat and moisture within the urban areas. The model solves for the wind flow, the temperature and relative humidity in the air, and the temperature and moisture content in building materials (Figure 1). The distribution of wind-driven rain (WDR) intensity is calculated using an Eulerian multiphase model (Kubilay et al. 2014). Direct and diffuse solar radiation as well as thermal radiation with diffuse reflections are taken into account. The model allows for the detailed spatial analysis of the cooling effect on the surfaces and in the air, as well as for the different contributions to cooling, such as shading, convective cooling, sensible heat transfer due to rain and evaporation. Modeling the heat and mass transport in building materials can improve the understanding in regards to the heat stored in urban areas during daytime due to solar heat flux and the heat released during nighttime.

The proposed approach is used in a case study composed of an isolated three-dimensional street canyon. Microclimatic conditions within the street canyon under dry and wet conditions are compared. The influence of materials with diverse heat and mass transport properties on the evaporative cooling and surface temperatures is investigated. Specifically, the impact of rain on microclimate is investigated by comparing the resulting thermal conditions following a rain event to those of a dry day.
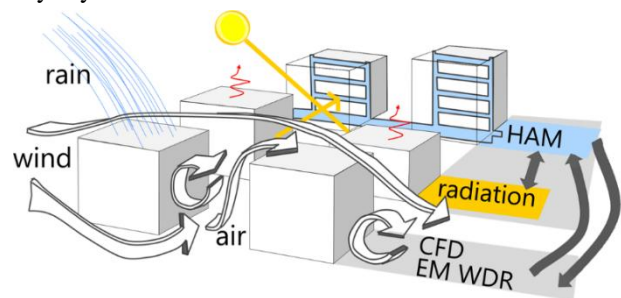

Figure 1. Schematic of the main physics implemented in the coupled urban microclimate model.

Description of the case study

The case study considers the microclimatic conditions in an isolated street canyon on a typical summer day. Both buildings have the dimensions of height × length × width of $10 \times 10 \times 50$ m³. The computational domain as well as the orientation of the buildings with respect to the wind-flow direction and the sun is given in Figure 2a. The reference wind speed is set to 5 m/s at the building height and wind direction is from due west. For simplicity, wind speed and direction are assumed constant during the day. After sunrise, the solar rays first hit the leeward wall of the street canyon, while the street-canyon ground and the windward wall are shaded. Around the solar noon, the ground is receiving solar rays with an angle close to the normal. Later, the solar rays hit the windward wall of the street canyon.

Initially, the domain is subjected to meteorological conditions on a dry day without rain, at typical early summer, with moderate ambient temperatures. The meteorological data are based on a typical meteorological year (Meteonorm 2000) and total solar radiation intensity for clear sky (ASHRAE 1985) for 21st of June in the city of Zurich, Switzerland. Figure 2b shows the variations of ambient temperature and relative humidity as well as the solar radiation. The maximum ambient temperature is around 19°C, while the minimum is around 11°C. The relative humidity varies between 62% and 86%.
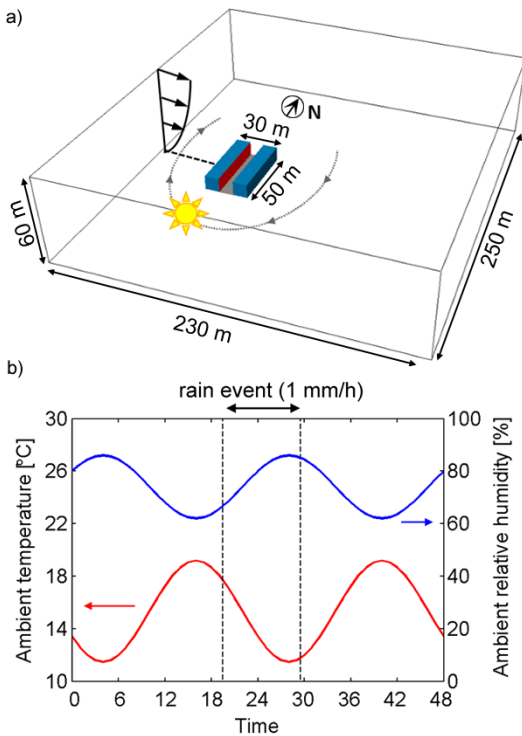

Figure 2. a) Computational domain and orientation of the street canyon with respect to wind direction and the sun. b) The daily variation of ambient air temperature and relative humidity.

For the wet case, a simple uniform rain event is considered. The rain event starts at sunset and continues uniformly until sunrise for a duration of 10 hours (between 19:30 and 05:30) as indicated in Figure 2b. The horizontal rainfall intensity, i.e. the rainfall intensity through a horizontal plane, is assumed to be constant at 1 mm/h. The distribution of WDR intensity on surfaces is calculated using an Eulerian multiphase model. All the other conditions are the same as in the dry case. The initial values for the simulation of the rain event are the state at 19:30 calculated for the dry day. Afterwards, the simulations for the rainy case are run until the end of the following day.

The heat and moisture transport at the street-canyon surfaces, i.e. building facades and street, are coupled with the air flow. Therefore, the resulting WDR intensity at these surfaces is applied as an influx boundary condition. The schematic for the computational domain of the porous building materials in the street canyon is given in Figure 3. The leeward and windward walls of the street canyon are finished with an exterior layer of 0.09m thickness. The interior surfaces are modelled with a thermal resistance of 2.5 m²K/W. An indoor temperature of 20°C is chosen. The interior surfaces of the facades are assumed to be impermeable to moisture. The outer layer of the street-canyon ground has a thickness of 0.10 m. Beneath this layer, soil with a depth of 1.90 m is located. Soil is chosen to consist of a balanced proportion of sand, silt and clay. Soil temperature at the bottom is set to 10°C. The bottom surface of the soil layer is assumed to be impermeable to moisture. The lateral boundaries of the porous material layers are assumed to be adiabatic and impermeable.
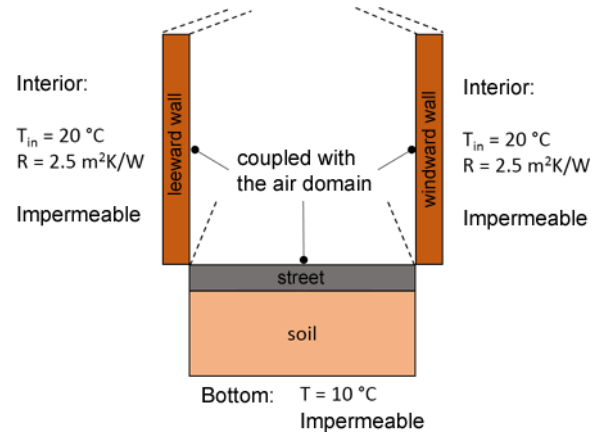

Figure 3. Configuration of the 3D models for the street-canyon facades and the ground (not to scale).

Three different material configurations are considered in the case study. For all configurations, the leeward and windward walls are assumed to consist of clay brick. Different materials are considered for the street surface. In case A, the outer layer of the street is considered as concrete, which is chosen as it has very limited moisture absorption. In case B, the outer layer is composed of bare soil, resulting in a total soil depth of 2 m. Concrete reaches capillary moisture content at very low relative humidity (large capillary pressure). In return, soil can hold more moisture and has significantly higher liquid

permeability as the relative humidity increases as shown by the moisture retention and the liquid permeability curves in Figure 4. Thermal properties for the dry materials are given in Table 1. The maximum moisture content in the building materials is the capillary saturated moisture content. In the present study, film runoff on the exterior surfaces is not modelled.
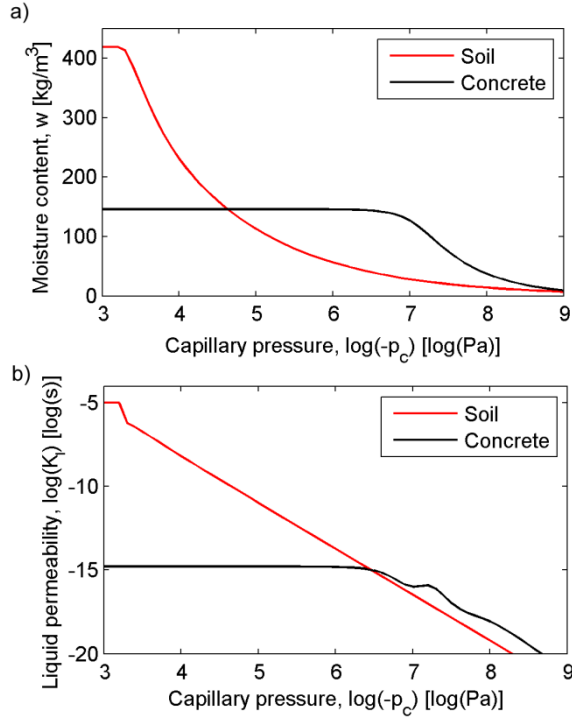

Figure 4. a) Wetting moisture retention and b) liquid permeability for soil and concrete.

Table 1: Thermal properties of the dry materials used in porous media

Material	Density [kg/m³]	Specific heat [J/kgK]	Thermal conductivity [W/mK]
Brick	1600	1000	0.68
Concrete	2280	800	1.50
Soil	1150	650	1.50

The moisture content for the street-canyon facades is initialized with 60% relative humidity. The street-canyon ground is initialized with a moisture saturation of 10% and the outer layer is let to dry. The simulations for the dry case have been run initially for several days using the meteorological data for 21st of June as boundary conditions until the conditions reach a daily thermal cycle that is independent from the initial values.

The outer surfaces of the facades and the ground have an emissivity of 0.9 and an albedo of 0.4, independent of the surface material. In the present paper, the focus is on the moisture absorption of different materials and its influence on evaporative cooling. In reality, materials with different albedos will change the absorbed solar radiation and, therefore, have an influence on drying rate.

Coupled multi-transport model

Conjugate heat and mass transport in air and building materials are coupled in such a way that the steady Reynolds-averaged Navier-Stokes (RANS) equations are solved together with unsteady equations of heat and moisture transfer in building materials for each timestep in a daily cycle of ambient temperature and relative humidity on a typical day. This approach is valid due to the fact that the time scale of transport in building materials is larger than the time scale of transport in air. A similar approach is applied by Saneinejad et al. (2014) to assess thermal comfort while neglecting 3D effects. The following subsections give the governing equations and the numerical settings used in each submodel.

Wind flow

Steady RANS with the standard k-ε model (Launder and Sharma 1974) is chosen for wind-flow simulations. In addition to RANS k-ε equations, governing equations for heat (as an active scalar) and moisture (as a passive scalar) transport are solved in the air domain. Buoyancy is modelled by taking into account the effect of temperature on air density.

The inlet profiles of mean wind speed, turbulence kinetic energy k and turbulence dissipation rate ε are shown in Equation 1 following the definitions by Richards and Hoxey (1993), where $U(y)$ denotes the horizontal wind speed at height y, u^*_{ABL} the atmospheric-boundary-layer friction velocity, y_0 the aerodynamic roughness length, κ the von Karman constant and C_μ a model constant. The log-law expression for the inlet mean wind speed profile is characterized by the normalized expression $u^*_{ABL}/U = 0.072$ and y_0 is chosen 0.03 m, representing a levelled country with low vegetation, e.g. grass, and isolated obstacles (Wieringa 1992).

$$U(y) = \frac{u^*_{ABL}}{\kappa} \ln\left(\frac{y + y_0}{y_0}\right)$$
$$k(y) = \frac{u^{*2}_{ABL}}{\sqrt{C_\mu}}$$
$$\varepsilon(y) = \frac{u^{*3}_{ABL}}{\kappa(y + y_0)}$$

(1)

For wall treatment, standard wall functions by Launder and Sharma (1974) are used. For the ground surface, sand-grain roughness modification is considered. The equivalent sand-grain roughness height, k_s, is taken to be 0.03 m and the roughness constant, C_s, is set as 9.793. Building surfaces are assumed smooth. A constant static gauge pressure of 0 Pa is used at the outlet boundary. Symmetry conditions are applied on both sides of the domain.

Wind-driven rain (WDR)

WDR intensity is calculated with an Eulerian multiphase (EM) model (Kubilay et al. 2014). In the EM model, the rain phase is regarded as a continuum, as is the wind phase. Each raindrop-size class is treated as a different phase, as raindrops of similar size will interact with the

wind-flow field in a similar way. Rain phase calculations are one-way coupled with the air phase, given that the effect of raindrops on the wind flow is ignored. For each rain phase, the following continuity and momentum equations are solved:

$$\frac{\partial \alpha_d}{\partial t} + \frac{\partial \alpha_d \overline{u_{d,j}}}{\partial x_j} = 0 \tag{2}$$

$$\frac{\partial \alpha_d \overline{u_{d,i}}}{\partial t} + \frac{\partial \alpha_d \overline{u_{d,i}} \, \overline{u_{d,j}}}{\partial x_j} + \frac{\partial \alpha_d \overline{u'_{d,i} u'_{d,j}}}{\partial x_j} = \tag{3}$$

$$\alpha_d g_i + \alpha_d \frac{3\mu_a}{\rho_w d^2} \frac{C_d \operatorname{Re}_R}{4} \left(\overline{u_i} - \overline{u_{d,i}} \right)$$

where α_d is the phase fraction of rain phase d, which represents a specific class of raindrop size, $u_{d,j}$ denotes the velocity component of rain phase d, u_i the velocity component of wind in direction i, ρ_w the density of the raindrops, μ_a the dynamic air viscosity, g the gravitational acceleration, C_d the drag coefficient. Re_R denotes the relative Reynolds number calculated using the relative velocity between the air and rain phases. The third term on the left-hand side in Equation 3 corresponds to the turbulent mass flux, which is the transport of mass due to turbulent motions in the flow. Turbulent dispersion of droplets is due to these turbulent motions. By defining a response coefficient, velocity fluctuations in rain phases can be related to the velocity fluctuations in the wind (Kubilay et al. 2015a).

This model provides the distribution of WDR intensity on all the surfaces of the computational domain, which is influenced by building geometry, position on the surface, wind speed, wind direction and rainfall intensity. The model is validated against field measurements on various geometries during rain events with different characteristics (Kubilay et al. 2014, 2015b).

Coupled heat and moisture transport in building materials

Absorption, transport and storage of heat and moisture are simulated within the building materials using coupled heat and moisture transport equations for porous media. A porous material consists of a solid material matrix and a pore space (porosity), which can be filled with gas (water vapour or dry air) or liquid. In the present study, the continuum modelling approach is applied, where the different phases are not distinguished separately at a certain point in the material but, instead, the macroscopic behaviour of the porous material is modelled.

The governing equations for moisture transport within the porous domains are given in Equation 4a, where g_l and g_v denote liquid and vapour moisture transfer, which are defined in Equations 4b and 4c, respectively.

$$\frac{\partial w}{\partial p_c} \frac{\partial p_c}{\partial t} = -\nabla \left(g_l + g_v \right) \tag{4a}$$

$$g_l = -K_l \nabla p_c \tag{4b}$$

$$g_v = -\frac{\delta_v p_v}{\rho_l RT} \nabla p_c - \frac{\delta_v p_v}{\rho_l RT^2} (\rho_l L_v - p_c) \nabla T \tag{4c}$$

In Equations 4a-4c, w denotes moisture content, p_c capillary pressure, T absolute temperature, K_l the liquid permeability, δ_v the vapour permeability, p_v the vapour pressure, ρ_l the liquid density, R the gas constant and L_v the heat of vaporization. The derivative $\partial w/\partial p_c$ represents the moisture capacity, i.e. the derivative of the moisture retention curve which gives the moisture content w as a function of the capillary pressure p_c. K_l and δ_v are dependent on moisture content and are typically obtained by using experimental techniques.

The governing equations for heat transport within the porous domains are given in Equation 5a, where q_c and q_a denote conductive and advective heat transfer and are defined in Equations 5b and 5c, respectively.

$$\left(c_0 \rho_0 + c_l w \right) \frac{\partial T}{\partial t} + \left(c_l T \frac{\partial w}{\partial p_c} \right) \frac{\partial p_c}{\partial t} = -\nabla \left(q_c + q_a \right) \tag{5a}$$

$$q_c = -\lambda \nabla T \tag{5b}$$

$$q_a = (c_l T) g_l + (c_v T + L_v) g_v \tag{5c}$$

In Equations 5a-5c, c_0 denotes the specific heat of the dry material, c_v the specific heat of water vapour, c_l the specific heat of liquid water, ρ_0 density of the dry material, and λ the thermal conductivity. The advective heat transfer, q_a, represents advective heat flow due to vapour and liquid flow including latent heat transport. A detailed description of the derivation of the governing equations and the underlying assumptions can be found in Janssen et al. (2007).

The heat and moisture fluxes calculated in the air domain are set as boundary conditions for the exterior surfaces of the building materials. The moisture exchange at the exterior surfaces of building materials comprises the convective vapour exchange and the rain flux. The heat exchange comprises the convective heat transfer, the radiative heat transfer, the sensible heat transfer due to rain and the latent and sensible heat transfer due to vapour exchange. The rain flux and the radiative heat flux are calculated by the respective submodels. The convective heat and mass fluxes are the values obtained in the CFD calculation.

The model is validated with existing results of moisture uptake experiments on porous stones (Derluyn et al. 2013) and verified by comparing with HAMSTAD (Heat Air and Moisture STAndards Development) benchmark cases (Hagentoft et al. 2004) which are specifically developed for moisture transport in building materials.

Radiative heat transfer

Short-wave (solar) and long-wave (thermal) radiation heat transfer are modelled based on a radiosity approach. The model considers the radiation exchange between the domain surfaces and with the sky. Air is considered as a non-participating medium, i.e. absorption, scattering and emission of radiation by air are neglected. All surfaces

are assumed opaque to both long-wave and short-wave radiation, i.e. windows on building facades are not considered and, therefore, transmissivity is zero. The model further assumes that surfaces are gray and diffuse, i.e. emissivity and absorptivity are equal and independent of wavelength and direction. The following equations are solved to calculate the net radiative heat flux at boundaries:

$$q_{out,k}^{L} = \varepsilon_k \sigma T_k^4 + \rho_k \sum_{j=1}^{N} F_{kj} q_{out,j}^{L} \qquad (6)$$

$$q_{out,k}^{S} = -(1-a_k) I_{sol} + a_k \sum_{j=1}^{N} F_{kj} q_{out,j}^{S} \qquad (7)$$

where $q_{out,k}^{L}$ denotes the energy leaving the surface k due to long-wave radiation and $q_{out,k}^{S}$ due to short-wave radiation. ε_k denotes the emissivity of surface k, σ the Stephan-Boltzmann constant, T_k the surface temperature, ρ_k the reflectivity of surface k, a_k the albedo, i.e. short-wave reflectivity, of surface k. F_{kj} denotes the view factor between surfaces k and j, I_{sol} the total solar radiation incoming to surface k.

View factors between surfaces, i.e. the fraction of energy leaving a surface that is incident on another, are calculated once at the beginning of the simulation. Incoming solar radiation is composed of direct and diffuse components, both of which depend on the time of the year and the location (ASHRAE 1985). The direct component of incoming solar radiation is calculated with ray tracing and takes into account the variation of shading and incidence angle over the day, here June 21st. The sky temperature is calculated based on the cloud cover and the ambient temperature (Cole 1976).

The system of linear equations in Equations 6 and 7 allows for an infinite number of reflections between surfaces. Reflections due to both long-wave and short-wave radiation are assumed to be diffuse.

Solver settings

OpenFOAM® 2.4 is used as the CFD solver with three main add-ons implemented by the authors: the WDR solver, the solar radiation model and the governing equations for the coupled heat and moisture transport in porous materials. The coupling between the air and porous domains is performed by sequentially solving the steady governing equations in the air and the unsteady governing equations in the porous domains for each exchange timestep. Exchange timestep is defined as the timestep where the information is exchanged at the air/surface interfaces (Saneinejad et al. 2014). During the transient simulation within the solid porous materials, the solution of air domain remains constant. Therefore, the exchange timestep is chosen to be 10 min in this study, as an hourly exchange time step is too long.

For each exchange timestep, first, the steady air flow is solved. The pressure-velocity coupling for the wind-flow solution is done with the Semi-Implicit Method for Pressure Linked Equations (SIMPLE) algorithm. Second

order discretization schemes are used for both the convection terms and the viscous terms of the governing equations. The simulations in the air domain are terminated when all the scaled residuals reach a value below 10^{-5} for all velocity components, turbulence terms and continuity; 10^{-4} for heat and moisture. Afterwards, the calculated heat and moisture fluxes at the street-canyon boundaries in the air domain are applied as boundary conditions in the coupled porous domains representing the building materials. Transient heat and mass transport in porous domains are simulated using adaptive timesteps (Janssen et al. 2007). For this, an internal iteration is performed, during which the thermal radiative heat fluxes are updated until temperature and moisture content values converge. Finally, the new values for temperature and moisture at the boundaries of the porous domain are used to solve the steady air flow for the next exchange timestep.

Results

Figure 5 shows the daily variation of exterior surface temperatures at the centre and at the side of the street-canyon surfaces during a dry day for case A. The results show large spatial gradients in street-canyon surface temperatures. For both night and day times, the highest surface temperatures are observed at the centre of the surfaces. The order for the occurrence of peak temperatures follow the movement of the sun, i.e. first the leeward facade and, then, the street and windward facade.
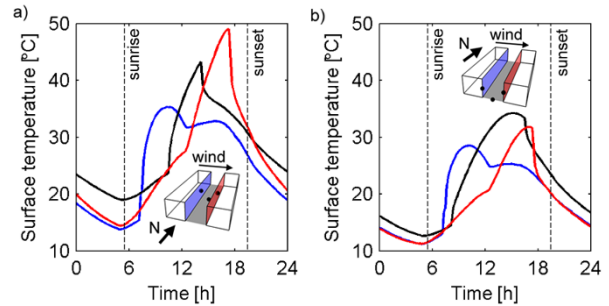

Figure 5. Surface temperature for a point in the middle of the surfaces, a) at the centre and b) at the side of the street canyon, for case A, i.e. with concrete as pavement.
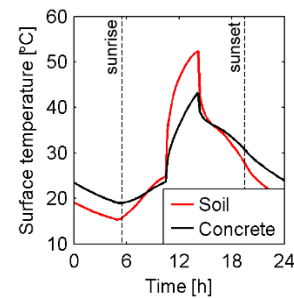

Figure 6. Surface temperature at a point at the centre of street comparing cases A (concrete) and B (bare soil).

Figure 6 compares the surface temperatures for the street surface for cases A and B. A larger temperature difference is observed for case B with soil, with higher temperature during day and lower temperature during

night. For the dry case, concrete has a larger heat capacity (ρc), which leads to slower change in temperature. For both cases A and B, the surface temperatures are found to be very similar for the windward and leeward facades since the material is the same (clay brick) for both cases.
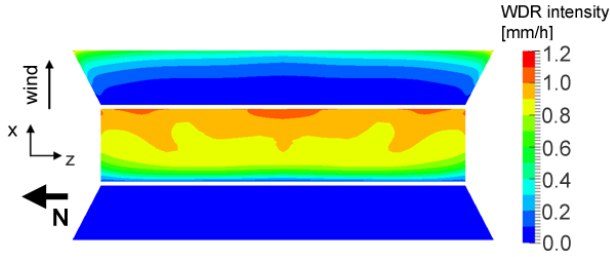

Figure 7. The distribution of WDR intensity on the street-canyon surfaces (top: windward facade, middle: street, bottom: leeward facade) with a perspective view from top.

The street surface is exposed to the highest amount of WDR intensity. Figure 7 shows the distribution of time-averaged WDR intensity on the surfaces of the street canyon for a rainfall intensity of 1 mm/h. The windward and leeward facades as well as the street surface are shown using a perspective view from above the street canyon. The surface-averaged WDR intensity is 0.81 mm/h on the street, 0.16 mm/h on the windward facade, whereas the leeward facade is sheltered from rain. The spatial gradient on the street surface is due to different inertia of different raindrop sizes. Sheltering effect is different for raindrops with different inertia. There is also a large gradient of WDR intensity on the windward facade, where the upper and side edges are exposed to higher WDR amounts. This is a result of higher wind speed around the edges of the building.

Figure 8 shows the variation of exterior surface temperature comparing the dry and wet cases at the centre of street surface. As the rain event starts, a decrease in the surface temperature is observed for both materials due to evaporative cooling and sensible heat transfer due to rain. The initial temperature decrease is similar for both materials and this effect keeps on during the whole rain event. Once the rain event stops, the surface temperatures stay about 5°C below the dry case for both materials and a sharp decrease in surface moisture contents is observed for both materials. At the time the peak temperature occurs (t = 39h), the surface moisture content for concrete is already almost down to its value for the dry case. In fact, the penetration depth during the rain event is much smaller for concrete (about 5-6 mm). Due to this reason, the impact of the rain event at the peak temperature is only 2°C. On the other hand, a difference larger than 10°C is observed for the surface temperature of soil.
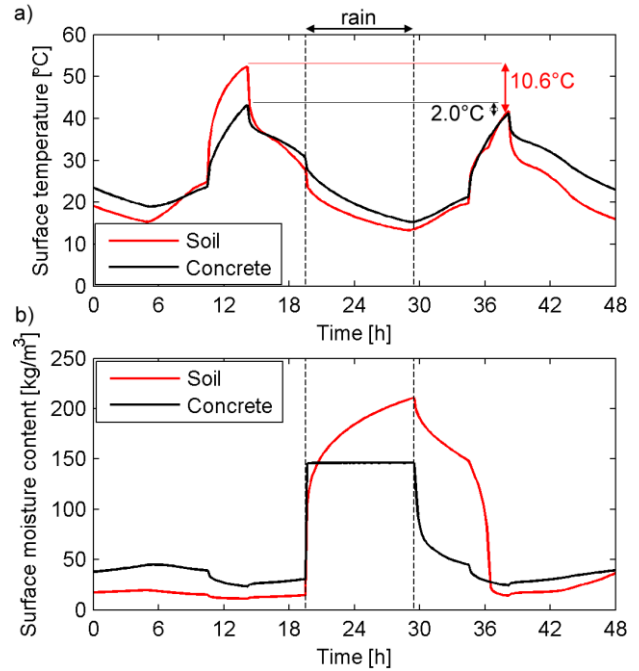

Figure 8. Variation of a) surface temperature and b) moisture content at a point at the centre of the street surface.

Figure 9 evaluates the impact of evaporative cooling for both materials on the street by comparing the differences in surface temperature of the wet and dry cases. Once the rain event stops, the decrease in temperature starts to increase for soil. As the solar radiation enhances the evaporation from the soil surface, the decrease in surface temperature gets as large as 15°C. On the other hand, for concrete, the difference in surface temperature gets smaller once the rain event stops. The reason for this is the fact that concrete absorbs a smaller amount of rainwater, which results in a slower drying rate.
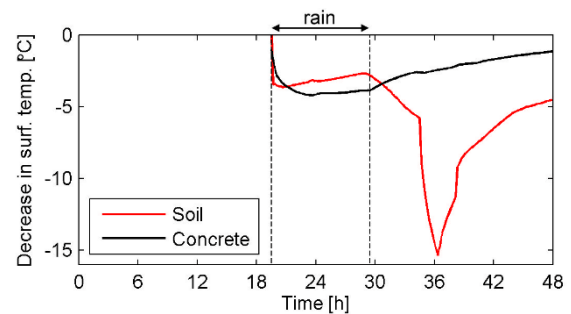

Figure 9. Difference of surface temperature between rainy and dry cases at a point at the centre of the street surface.

Discussion

The present study focuses on the impact of materials with different moisture permeability and capacity on the evaporative cooling after a simple rain event. Specifically, the effect of two materials with opposite moisture characteristics is compared at the street level: concrete and soil. The study neglects variations in wind speed and wind direction during the day, by keeping

them constant. Furthermore, this study does not take into account the droplet physics after impact such as spreading, splashing, film forming or run-off. As the capillary moisture content at the surface of concrete is reached during the rain event, it is assumed all the excess rainwater is removed from the surface. In reality, thin surface film may stay on the street surface, e.g. rain puddles, which would further delay the drying of concrete.

In general, RANS k-ε models have drawbacks related to the overprediction of the size of the wake and the location of reattachment due to the underestimation of turbulence kinetic energy in the wake of the building (Murakami 1993). On the other hand, more complicated turbulence models such as large eddy simulation (LES) result in a higher computational cost, especially considering the three-dimensional coupling and daily simulations intended in the present modeling approach. An unsteady RANS simulation would also likely increase the computation time for the air domain. Note also that the standard wall functions have limitations in terms of the accuracy of predicted heat flux and several studies suggested improvements by modifying the turbulent Prandtl number (Defraeye et al. 2011; Allegrini et al. 2012).

Conclusion

In this study, a fully-integrated 3D numerical urban microclimate model is developed and presented. For this, wind flow in the air is solved together with heat and moisture transport both in the air and in the porous building materials, as well as the solar and thermal radiation with exchanges. Steady RANS simulations for air flow are coupled with unsteady heat and moisture transfer in building materials for each exchange timestep. Spatial distribution of surface wetting due to WDR is calculated using an Eulerian multiphase model.

The presented model provides detailed spatial distribution of heat and moisture, allowing the study of different contributions to cooling, e.g. convective cooling, sensible heat transfer due to rain, evaporation, as well as the comparison of heat storage and heat-removal and thermal comfort for different conditions.

Further work is planned to study especially the influence of vegetation, e.g. trees, green roofs. Next steps will implement more accurate wind-flow conditions based on actual meteorological data, take into account different orientations with respect to the sun and rain, couple with comfort models and study the influences of vegetation. Also, the effect of different surface albedos on the thermal comfort throughout the day needs to be investigated.

Acknowledgement

References

Allegrini, J., Dorer, B., Defraeye, T., and J. Carmeliet. (2012). An adaptive temperature wall function for mixed convective flows at exterior surfaces of buildings in street canyons. *Build Environ 49*, 55–66.

ASHRAE (1985). ASHRAE Handbook - Fundamentals: American Society of Heating, Refrigerating and Air-Conditioning Engineers Inc.

Cole, R.J. (1976). The longwave radiative environment around buildings. *Build Environ 11*, 3–13.

Defraeye, T., Blocken, B., and J. Carmeliet. (2011). An adjusted temperature wall function for turbulent forced convective heat transfer for bluff bodies in the atmospheric boundary layer. *Build Environ 46*, 2130–2141.

Derluyn, H., Griffa, M., Mannes, D., Jerjen, I., Dewanckele, J., Vontobel, P., Sheppard, A., et al. 2013. (2013). Characterizing saline uptake and salt distributions in porous limestone with neutron radiography and X-ray micro-tomography. *J Build Phys 36*, 353–374.

Hagentoft, C.-E., Kalagasidis, A.S., Adl-Zarrabi, B., Roels, S., Carmeliet, J., Hens, H., Grunewald, J., et al. (2004). Assessment Method of Numerical Prediction Models for Combined Heat, Air and Moisture Transfer in Building Components: Benchmarks for One-dimensional Cases. *J Therm Envel Build Sci 27*, 327–352.

Janssen, H., Blocken, B. and J. Carmeliet (2007). Conservative modelling of the moisture and heat transfer in building components under atmospheric excitation. *Int J Heat Mass Tran 50*, 1128–1140.

Kubilay, A., Derome, D., Blocken, B. and J. Carmeliet (2014). Numerical simulations of wind-driven rain on an array of low-rise cubic buildings and validation by field measurements. *Build Environ 81*, 283–295.

Kubilay, A., Derome, D., Blocken, B. and J. Carmeliet (2015a). Numerical modeling of turbulent dispersion for wind-driven rain on building facades. *Environ Fluid Mech 15(1)*, 109–133.

Kubilay, A., Derome, D., Blocken, B. and J. Carmeliet (2015b). Wind-driven rain on two parallel wide buildings: field measurements and CFD simulations. *J Wind Eng Ind Aerod 146*, 11–28.

Launder, B.E., and B.I. Sharma (1974). Application of the Energy-Dissipation Model of Turbulence to the Calculation of Flow Near a Spinning Disc. *Lett Heat Mass Trans 1(2)*, 131–138.

Meteonorm (2000). Global meteorological database for solar energy and applied climatology. Bern, Switzerland, Meteotest.

Mirzaei, P.A., and F. Haghighat (2010). Approaches to study Urban Heat Island – Abilities and limitations. *Build Environ 45(10)*, 2192–2201.

Moonen, P., Defraeye, T.W.J., Dorer, V., Blocken, B. and J. Carmeliet (2012). Urban physics: effect of the microclimate on comfort, health and energy demand. *Front Arch Res 1(3)*, 197–228.

Murakami, S. (1993). Comparison of various turbulence models applied to a bluff-body. *J Wind Eng Ind Aerod 46*, 21–36.

Richards, P.J., and R.P. Hoxey (1993). Appropriate boundary conditions for computational wind engineering models using the k-ε turbulence model. *J Wind Eng Ind Aerod 46-47*, 145–153.

Saneinejad, S., Moonen, P. and J. Carmeliet (2014). Coupled CFD, radiation and porous media model for evaluating the micro-climate in an urban environment. *J Wind Eng Ind Aerod 128*, 1–11.

Toparlar, Y., Blocken, B., Vos, P., van Heijst, G.J.F., Janssen, W.D., van Hooff, T., Montazeri, H., and H.J.P. Timmermans (2015). CFD simulation and validation of urban microclimate: A case study for Bergpolder Zuid, Rotterdam. *Build Environ 83*, 79–90.

Wieringa, J. (1992). Updating the Davenport roughness classification. *J Wind Eng Ind Aerod 41*, 357–368.